PASJ: Publ. Astron. Soc. Japan , 1–??,

Outburst and Post-Outburst Active Phase of the Black Hole X-ray Binary V4641 Sgr in 2002

Makoto Uemura[1], Taichi Kato[1], Ryoko Ishioka[1], Kenji Tanabe[2], Ken'ichi Torii[3], Roland Santallo[4], Berto Monard[5], Craig B. Markwardt[6], Jean H. Swank[7], Robert J. Sault[8], Jean-Pierre Macquart[9], Michael Linnolt[10], Seiichiro Kiyota[11], Rod Stubbings[12], Peter Nelson[13], Tom Richards[14], Charles Bailyn[15], Doug West[16], Gianluca Masi[17], Atsushi Miyashita[18], Yasuo Sano[19], and Toni Scarmato[20]

[1]*Department of Astronomy, Faculty of Science, Kyoto University, Sakyou-ku, Kyoto 606-8502*
uemura@kusastro.kyoto-u.ac.jp

[2]*Department of Biosphere-Geosphere Systems, Faculty of Informatics, Okayama University of Science, Ridaicho 1-1, Okayama 700-0005*

[3]*Cosmic Radiation Laboratory, RIKEN (Institute of Physical and Chemical Research), 2-1, Hirosawa, Wako, Saitama 351-0198*

[4]*Southern Stars Observatory IAU # 930, Tahiti French Polynesia*

[5]*Bronberg Observatory, PO Box 11426, Tiegerpoort 0056, South Africa*

[6]*Department of Astronomy, University of Maryland, College Park, MD 20742, USA*

[7]*Laboratory for High Energy Astrophysics, NASA Goddard Space Flight Center, Mail Code 662, Greenbelt, MD 20771, USA*

[8]*Australia Telescope National Facility, Narrabri, NSW 2390, Australia*

[9]*Kapteyn Astronomical Institute, University of Groningen, Postbus 800, 9700 AV Groningen, The Netherlands*

[10]*PO Box 11401, Honolulu, HI 96828, USA*

[11]*Variable Star Observers League in Japan (VSOLJ); Center for Balcony Astrophysics, 1-401-810 Azuma, Tsukuba 305-0031*

[12]*19 Greenland Drive, Drouin 3818, Victoria, Australia*

[13]*RMB 2493, Ellinbank 3820, Australia*

[14]*Woodridge Observatory, 8 Diosma Rd, Eltham, Vic 3095, Australia*

[15]*Department of Astronomy, Yale University, P.O. Box 208101, New Haven, CT 06520-8101, USA*

[16]*West Skies Observatory, P.O. Box 517, Derby, KS 67037, USA.*

[17]*Via Madonna de Loco, 47, 03023 Ceccano (FR), Italy*

[18]*Seikei High School, 3-10-13 Kita-machi, Kichijouji, Musashino, Tokyo 180-8633*

[19]*VSOLJ, 3-1-5 Nishi Juni-jou Minami, Nayoro, Hokkaido 096-0022*

[20]*via Cuppari 10, 89817 San Costantino di Briatico (VV), Calabria, Italy*

(Received 2002 0; accepted 2002 0)

Abstract

The black hole X-ray binary V4641 Sgr experienced an outburst in 2002 May which was detected at X-ray, optical, and radio wavelengths. The outburst lasted for only 6 days, but the object remained active for the next several months. Here we report on the detailed properties of light curves during the outburst and the post-outburst active phase. We reveal that rapid optical variations of ~ 100 s became more prominent when a thermal flare weakened and the optical spectrum flattened in the $I_{\rm c}$, $R_{\rm c}$, and V-band region. In conjunction with the flat spectrum in the radio range, this strongly indicates that the origin of rapid variations is not thermal emission, but synchrotron emission. Just after the outburst, we detected repeated flares at optical and X-ray wavelengths. The optical and X-ray light curves exhibited a strong correlation, with the X-rays, lagging by about 7 min. The X-ray lag can be understood in terms of a hot region propagating into the inner region of the accretion flow. The short X-ray lag, however, requires modifications of this simple scenario to account for the short propagation time. We also detected rapid optical variations with surprisingly high amplitude 50 days after the outburst, which we call optical flashes. During the most prominent optical flash, the object brightened by 1.2 mag only within 30 s. The released energy indicates that the emission source should be at the innermost region of the accretion flow.

Key words: accretion, accretion disks—stars: binaries: close—individual (V4641 Sagittarii)

1. Introduction

Black hole X-ray binaries are close binary systems which contain a stellar mass black hole of $\sim 10 M_\odot$ and a main sequence or an evolved secondary star (Tanaka, Lewin 1995). The gas from the secondary star forms an accretion disk around the black hole, which causes various types of variations (van der Klis 1989; O'Donoghue, Charles 1996). X-ray rapid variations are of interest because their short time scales of 0.1–1000 Hz indicate their emission originates from the inner region of the accretion flow (e.g. Morgan et al. 1997; Wei et al. 1997). The variations of the X-ray flux hence provide important clues concerning the physics of the accretion flow, and on the nature of the black holes themselves(Wei et al. 1998; Abramowicz 2001).

Optical rapid variations from black hole binaries have recently received attention as unique probes of accretion and jet physics (Kanbach et al. 2001; Uemura et al. 2002). Rapid optical variability was first detected in the black hole binary GX 339−4 during an optically very bright state ($V = 15.4$) in 1981, when it showed 20 s optical QPOs with relatively large amplitudes, of order 0.1 mag (Motch et al. 1982). QPOs of similar amplitude but a 190 s period were detected during an optically moderate brightness state (Steiman-Cameron et al. 1990). Smaller-amplitude QPOs, of order 0.01 mag, with periods of 7–16 s were also reported (Motch et al. 1985; Imamura et al. 1990; Steiman-Cameron et al. 1997). Another black hole binary, V404 Cyg, exhibited possible 0.7 mag, 10 min variations around the maximum of its X-ray nova outburst (Buie, Bond 1989; Wagner et al. 1989). The object again showed 3–10 min, 0.01 mag QPOs during the decline from the outburst (Gotthelf et al. 1991). XTE J1118+480 recently provided a rare opportunity to observe rapid variations simultaneously at optical and X-ray wavelengths (Kanbach et al. 2001). Its 0.1 mag optical variations on a time scale of seconds exhibited a strong correlation with X-ray variations, with a preceding optical dip (Kanbach et al. 2001; Spruit, Kanbach 2002). GX 339−4 exhibited similar optical dips, which were anticorrelated with the X-ray flares (Motch et al. 1983). These rapid optical variations tend to appear during the low/hard state. On the other hand, $\lesssim 30$ s variations are reported in both A0620-00 and X-ray Nova Mus 1991 even in the quiescent state (Hynes et al. 2003).

The optical emission is generally considered to be thermal emission near the outer portion of the accretion disk, where the temperature is relatively low, of order 10^4 K (Tanaka, Lewin 1995). The short-time scale of the rapid variations implies that the emission originates in the inner part of the accretion flow. The spectrum expected for an optically-thick, geometrically-thin disk (the so called standard disk) predicts that most of the released energy is observed in the X-ray range, and only weak optical emission is expected from such an inner region. The rapid optical variations should hence originate from a non-thermal source, and the most promising candidate for this emission mechanism is synchrotron radiation (Fabian et al. 1982; Kanbach et al. 2001).

It has been proposed that strong synchrotron emission can significantly contribute to the optical flux observed in black hole binaries. Fender (2001) proposes that the low/hard states of black hole binaries are characterized by self-absorbed synchrotron emission from jets observed at radio wavelengths. The synchrotron emission from jets is proposed to extend to the infrared, and possibly to the optical. In the case of large-scale jets, a near-infrared jet was directly imaged in GRS 1915+105 (Sams et al. 1996). The ~ 1000 s infrared variations in this object precede the radio variations, and are widely believed to be synchrotron flares associated with the jet (Mirabel et al. 1998). Magnetic flares at the inner accretion flow are another proposed source of strong synchrotron emission (Merloni et al. 2000).

V4641 Sgr is an X-ray binary system with an orbital period of 2.8 d, containing a secondary star of 5–8$M_\odot$ and a black hole of $\sim 9.6 M_\odot$ (Orosz et al. 2001). This object first received attention during a luminous outburst in 1999 September. Despite its high luminosity, $\sim 10^{39}$ erg s^{-1}, the duration of the outburst was quite short; it lasted a few hours in the X-ray range (Smith et al. 1999) and one day in the optical range (Uemura et al. 2002). This system also possesses highly relativistic jets, which were detected by radio observations during this outburst (Hjellming et al. 2000). The source's rapid state transitions make it an ideal candidate to study the relationship between the accretion flow and the jet with multi-wavelength observations (Mirabel et al. 1998; Eikenberry et al. 1998). Activity was also reported in the radio range in 2000,[1] which implies that V4641 Sgr experiences active states frequently, in common with GRS 1915+105, but unlike most typical black hole binaries whose quiescent states last for over ten years (Rao et al. 2000; Tanaka, Lewin 1995).

The most recent major outburst occurred in 2002 May. During this outburst, we detected optical short-term modulations, a part of which was reported in Uemura et al. (2002). Here we report the detailed features of V4641 Sgr during the 2002 May outburst and the post-outburst active phase. In the next section, we present a short summary of our observations. In section 3, we report the results of our observations. We then discuss the nature of the emission source during the active phase in section 4. The summary of this paper is presented in the final section.

2. Observation

We performed CCD photometric observations at 15 optical observatories from JD 2452397 to 2452569. The observations were typically performed with 30-cm class telescopes. The journal of our CCD observations is given in table 1. We used the standard reduction method for obtained images, and adjusted unfiltered CCD magnitude systems to the R_c-system with the same manner described

[1] ⟨http://vsnet.kusastro.kyoto-u.ac.jp/vsnet/Mail/vsnet-campaign-xray/msg00009.html, msg00011.html, msg00020.html⟩

in Uemura et al. (2002).

The X-ray data were taken by the RXTE Porportional Counter Array (PCA) using pointed observations from 24.15–28.65 May 2002 (UT). The PCA consists of five Proportional Counter Units (PCUs) which are sensitive in the 2–60 keV X-ray band (Jahoda et al. 1996). The fields of view of the five PCUs are restricted to 1° FWHM by hexagonal collimators which are coaligned (2.2° full width at zero response). Data were filtered using the standard procedures for bright sources recommended by the RXTE Guest Observer Facility. The total good time was approximately 36 ks. Data from the Standard2 mode were used, which have a time binning of 16 sec and moderate spectral resolution. Counts from the top detector layer in the energy range 2–10 keV were selected. Particle backgrounds were subtracted using the "CMVLE" model, and an additional estimated background of 1.0 mCrab due to galactic diffuse emission was also subtracted. The quoted X-ray flux values were found by dividing the total count rate by the number of active PCUs, and scaling to the mean PCA count rate of the Crab in the same energy band. The X-ray outburst consisted of a period of about 2 days from 24–26 May where the flux varied from approximately 5–50 mCrab, with large fluctuations on time scales of minutes. After 26.0 May, no significant persistent flux was detected, however there continued to be X-ray flares with peak fluxes as high as 36 mCrab.

Radio observations were performed with the Australia Telescope Compact Array (ATCA) on JD 2452419 and briefly again on the two subsequent days. The ATCA is an Earth-rotation aperture synthesis array, comprising six 22 m antennas which can be moved along an east-west track to give baselines up to 6 km (Frater, Brooks, & Whiteoak 1992). The source was observed at bands centered on frequencies of 1.384, 2.496, 4.800 and 8.640 GHz with 128 MHz bandwidth in two orthogonal polarizations.

3. Results

3.1. Outburst in 2002 May

The outburst in May is characterized by a short total duration of about 6 days and multiple peaks as reported in Uemura et al. (2002). The whole light curve of the outburst is shown in the panel (a) of figure 1. In this figure, we also show examples of rapid variations detected during the outburst in the panel (b), (c), (d), and (e). The abscissa is the time in JD and the ordinate is the $R_{\rm c}$ magnitude.

One day after the first visual detection of the outburst (11.5 mag on JD 2452414), the object was detected at a fainter level of 12.8 mag. A subsequent rapid brightening on JD 2452415 is shown in the panel (b). The light curve shows short-term fluctuations with a time scale of 100 s and with large amplitudes of 0.1–0.5 mag. After this epoch, both visual and CCD observations recorded a temporal fading of about 1 mag. The tail of the fading and the rapid recovering was detected by our time-series observation on JD 2452416, as shown in the panel (c). It is notable that the strong short-term fluctuations in the panel (b) almost disappeared during this phase. A regrowth of short-term variations can be seen at the end of the light curve in the panel (c). On JD 2452417, the object seems to have remained at a bright state at about 12 mag. The light curve in the panel (d) shows more rapid short-term variations of a time scale of ~ 30 s. It is also characterized by a broad dip around JD 2452417.58, during which the short-term variation was relatively weak. The object again experienced a temporal fading, and then quickly recovered. The light curve in early JD 2452418 (panel (e)) was dominated by several dips rather than the fluctuations seen in the panel (b) and (d). The duration of the dips were only about 500 s, and the deepest dip was about 0.7 mag. These dips were, however, not observed 0.1 day after this epoch. As can be seen in the panel (e), the light curve in the middle JD 2452418 shows rather smooth variations of ~ 1000 s.

The object reached the maximum of the outburst on JD 2452419. We succeeded in obtaining multi-color light curves just before the maximum. The left panel of figure 2 shows the resulting light curves of B, V, $R_{\rm c}$, and $I_{\rm c}$ bands. We divided the light curve into 16 bins of $\Delta t = 0.01$ d, as labeled in the figure, and calculated de-reddened, mean flux of each bin. The obtained spectral energy distributions (SEDs) are normalized with the $R_{\rm c}$-flux and shown in the right panel of figure 2. The de-reddening procedure was performed with $E(B-V) = 0.32$ reported in Orosz et al. (2001) and the relationship on $E(V-R_{\rm c})$ and $E(R_{\rm c}-I_{\rm c})$ reported in Taylor (1986).

The object experienced a large hump in all bands during the bin No. 1–6 in figure 2. The peak was in the bin No. 3, when the object became bluer, as can be seen in the right panel of figure 2. After the hump, short-term fluctuations with a time scale of 100 s became stronger (the bin No. 9, 11, and 12), as can be seen in B- and $R_{\rm c}$-band light curves. The V- and $I_{\rm c}$-band light curves are relatively sparse, however the rapid variations can be confirmed even in these bands. The SED during this phase is characterized by flat spectra in the V–$I_{\rm c}$ region with the probable excess of the $R_{\rm c}$-flux. The flat spectral component again weakened since the bin No. 13, when another brightening started. As can be seen from figure 1 and 2, the properties of rapid variations were drastically changed within a short period, which was typically a few hours.

Figure 3 shows the result of radio observations on JD 2452419, a part of which was simultaneously performed with the optical observation. The panel (a) and (b) describe the optical and radio variations, respectively. The light curve in the panel (a) is the optical one corrected with the extinction of $A_{R_{\rm c}} = 0.86$ which was estimated from $E(B-V) = 0.32$. In the panel (b), the filled circles, open circles, filled triangles, and open triangles denote the radio flux of 8.64, 4.80, 2.50, and 1.38 GHz, respectively. No polarization was detected above the 3 mJy level, except at 8.64 GHz on JD 2452419, where Stokes Q amplitude was observed to peak, with $Q = -16\,mJy$ as can be seen in the panel (c), and subsequently decay as the total intensity decayed. The SEDs in the radio range are shown in the panel (d) for the early six sets and (e) for the late

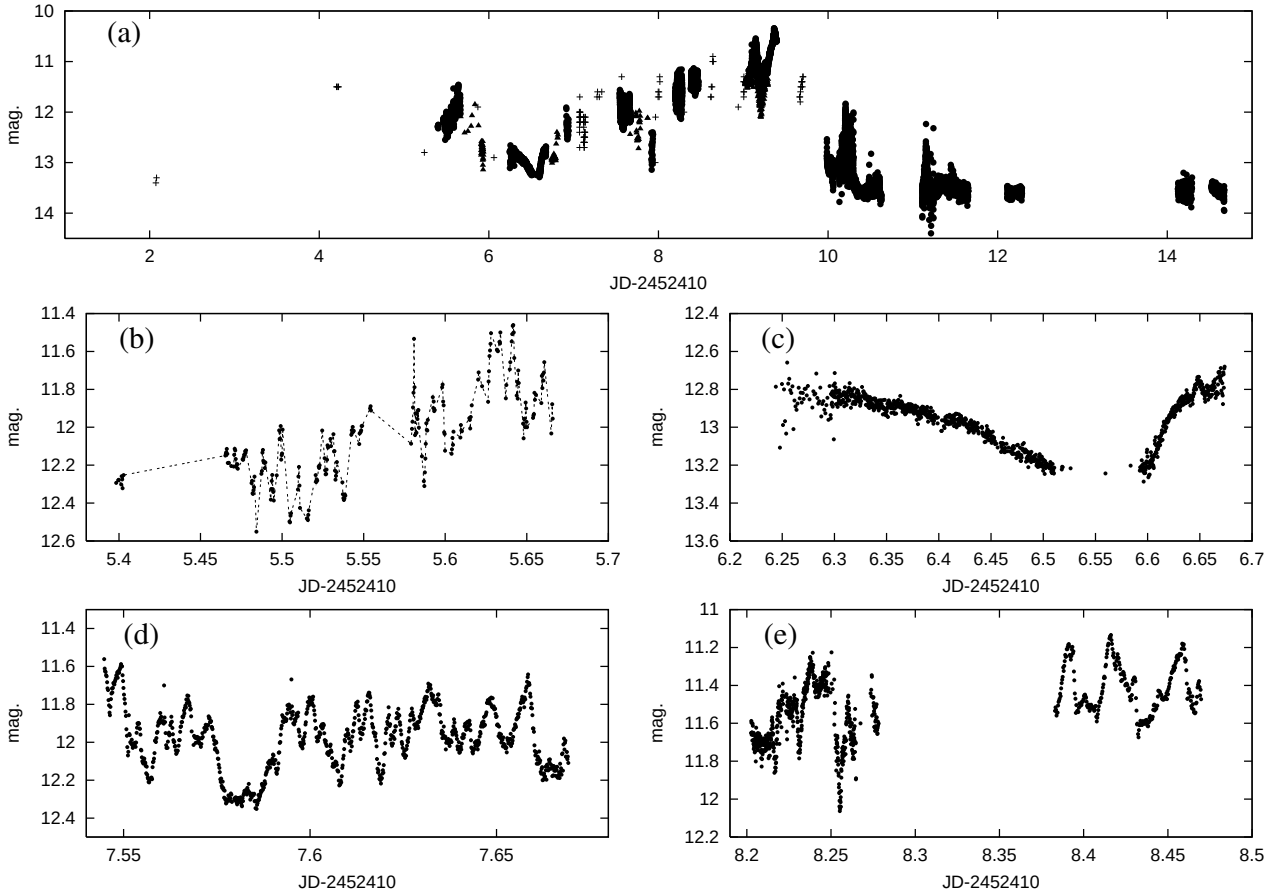

Fig. 1. Light curves during the May outburst. The abscissa and ordinate denote the time in JD and the R_c (and V in the panel (a)) magnitude, respectively. Panel (a): The whole light curve of the outburst. The filled circles and triangles are R_c- and V-magnitudes from our CCD observations, respectively. The crosses show visual observations reported to VSNET. Panel (b), (c), (d), and (e): Short-term variations during the outburst. Typical errors of each observation is 0.02 mag in the panel (b), 0.03 mag in the panel (c), 0.02 mag in the panel (d), 0.04 mag in the early observation in the panel (e), and 0.02 mag in the late observation in the panel (e). In the panel (b), we also show observations with a dotted line to show short-term variations more clearly.

four sets of observations. We calculated the spectral index α defined with $f_\nu \propto \nu^\alpha$, using all points of each epoch and three high frequency points (8.64, 4.80, and 2.50 Hz). The results are presented in table 2. We calculated two types of α because there is a possible break at 2–3 GHz in some SEDs.

As can be seen in figure 3 and table 2, the radio SEDs were first rapidly changing from almost flat spectra to highly inverted spectra. The spectral index reached at a surprisingly high level of about 0.8–1.0 around JD 2452419.1. In the late four spectra, the high-frequency flux gradually faded and the low-frequency flux almost remained constant. The spectra again became flat during this period. There is no clear correlation between the optical and the radio light curves within our available data.

The outburst was terminated by a sudden fading in the end of JD 2452419. The object then entered a post-outburst active phase. Both the radio flux and the spectral index rapidly decreased with time as shown in table 2 and figure 4.

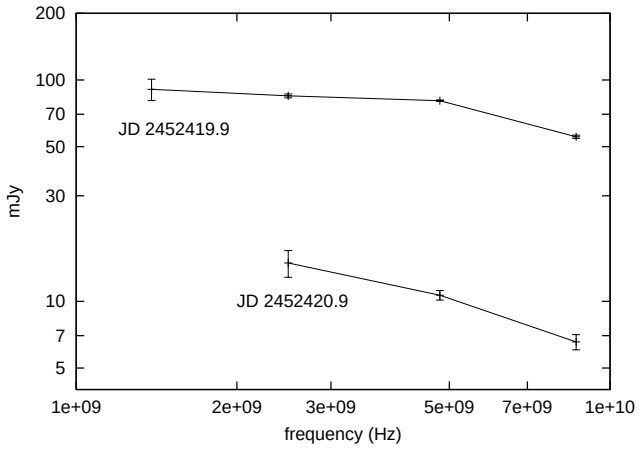

Fig. 4. Spectral energy distributions in the radio range just after the outburst. The abscissa and ordinate denote the frequency in Hz and the flux density in mJy, respectively. The upper and lower points are observations on JD 2452419.9 and JD 2452420.9, respectively. The error in the figure is the standard error.

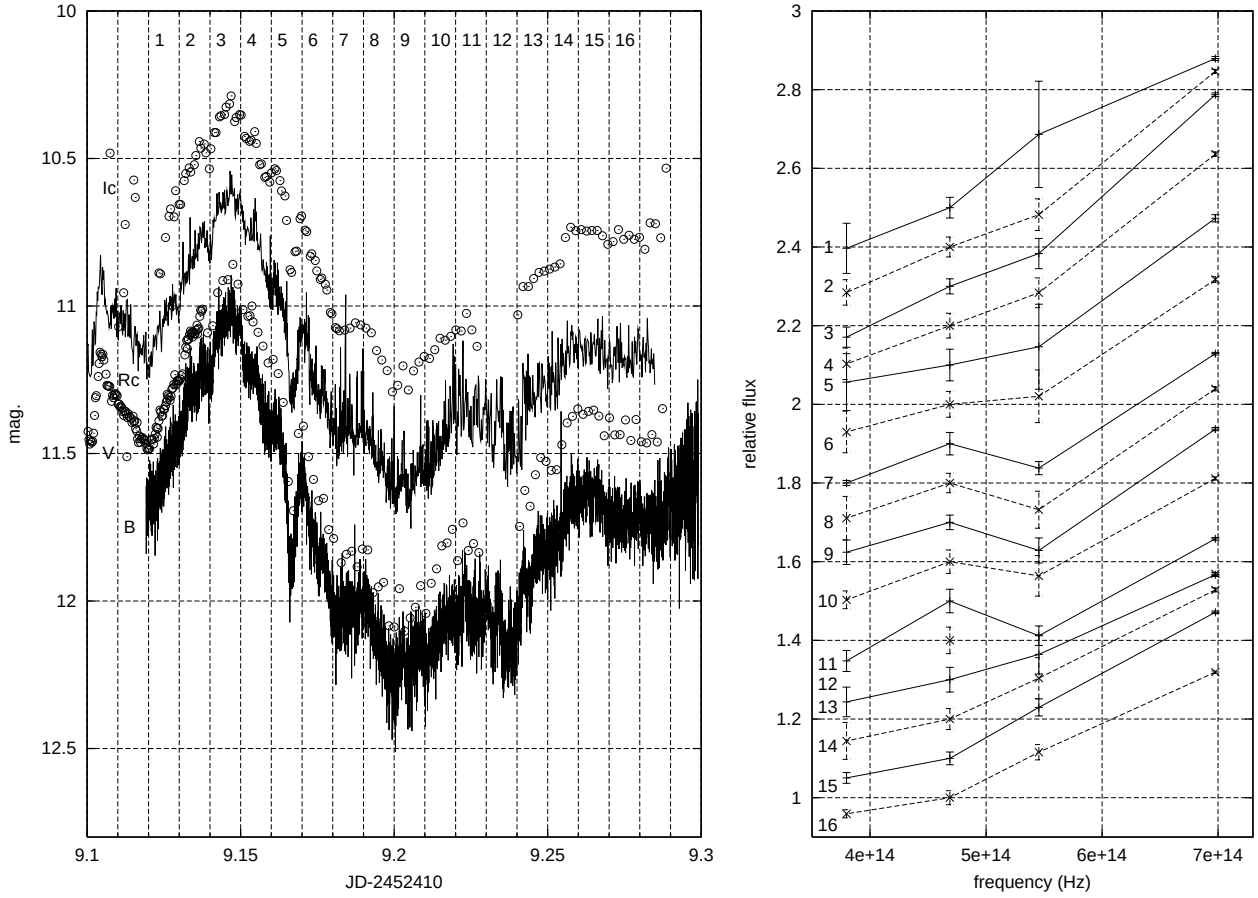

Fig. 2. B, V, R_c, and I_c simultaneous observations around the maximum of the outburst (JD 2452419). Left panel: Multi-color light curves. The abscissa and ordinate denote the time in JD and the magnitude, respectively. We show the light curves of I_c (open circles), R_c (line), V (open circles), and B (line) from top to bottom. Right panel: Time evolution of the de-reddened spectral energy distribution. The abscissa and ordinate denote the frequency in Hz and the relative flux in an arbitrary unit which is normalized at the R_c-band flux, respectively. The left-side number with each spectrum means the time bin of $\Delta t = 0.01$ d shown in the left panel. The error is the standard error in each bin. In the bin No. 12, only B and R_c-band observations are available. The R_c-band observation is shown as an isolated point in the right panel, and the B-band observation is roughly coincident with that of the bin No. 13.

3.2. Post-outburst active phase

3.2.1. Correlation between optical and X-ray emission just after the outburst

As reported in Uemura et al. (2002), our optical observation detected repeated flaring on JD 2452420, just after the outburst. This active phase has notable characteristics compared with known optical activities observed in other black hole binaries. First, the flares have large amplitudes of $\gtrsim 1$ mag (peak magnitudes ~ 11.9 mag) with short time scales. On their time scale, the e-folding time of rising or fading branches is calculated to be typically ~ 10 min, which is quite shorter than the time scale at the outermost region of the accretion disk. Second, the duration of this active phase was only about 3.5 hr, and it was suddenly terminated by a subsequent calm state. In the X-ray range, such rapid state transitions are well known in GRS 1915+105 (Greiner et al. 1996; Taam et al. 1997; Yadav et al. 1999). V4641 Sgr is a unique source in the point that such rapid state transitions were observed in the optical range.

During the active phase on JD 2452420, we succeeded in obtaining simultaneous light curves of optical (R_c and B) and X-ray emission. The light curves are shown in figure 5. The top, middle, and bottom panels are the light curve of R_c-band, B-band, and X-ray flux, respectively. In these light curves, the abscissa denotes the time in geocentric JD. The ordinate denotes the flux density in mJy for the optical data and in mCrab for the X-ray data.

Our observations demonstrate a clear correlation between the optical and the X-ray light curves. The first giant flare around the time of JD 2452420.19–2452420.23 in figure 5 is connected with a large double-peaked optical flare. Subsequent small optical flares during the same interval preceded several X-ray flares with profiles that resembled those observed at optical wavelengths. The time scale of the X-ray flare is shorter than that of the optical one. We calculated e-folding times of rising branches of this flare to be 12 ± 1 min in the optical range and 3 ± 1 min in the X-ray range. Compared with the optical light curve,

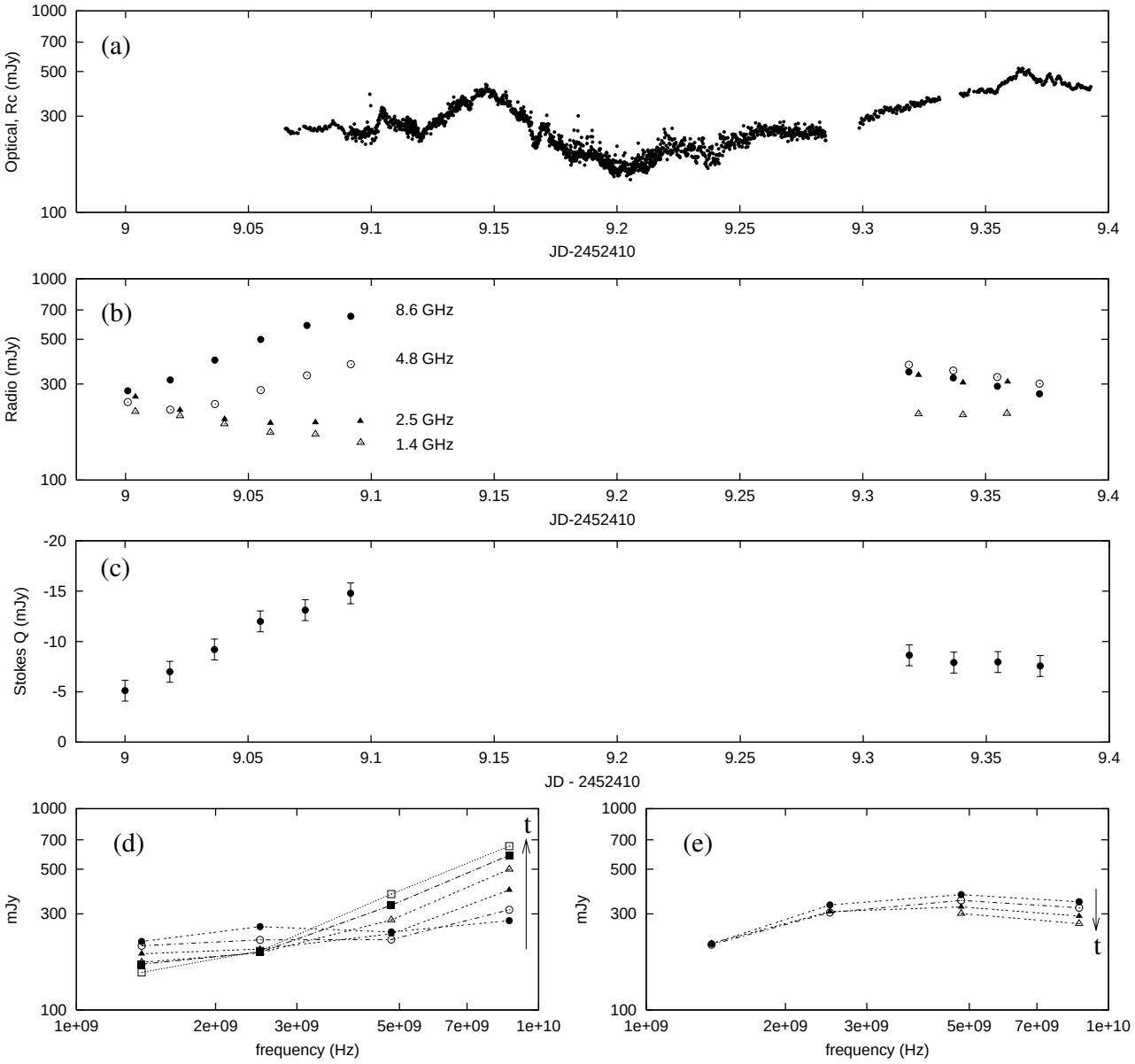

Fig. 3. Optical and radio observations around the maximum of the outburst (JD 2452419). Panel (a): Optical R_c-band light curve. The abscissa and ordinate are the time in JD and the flux density in mJy, respectively. Extinction corrections to the optical data were performed. Panel (b): Radio light curves. The abscissa and ordinate are same as the panel (a). The filled circles, the open circles, the filled triangles, and the open triangles denote the radio observations at 8.64, 4.8, 2.496, and 1.384 GHz, respectively. The standard errors of each point are smaller than the symbol size in the figure. Panel (c): Time evolution of the Stokes Q at 8.64 GHz. Panel (d) and (e): Time evolution of spectral energy distributions in the radio range. The abscissa and ordinate denote the frequency in Hz and the flux density in mJy, respectively. Observations in different epoch are shown with distinct symbols.

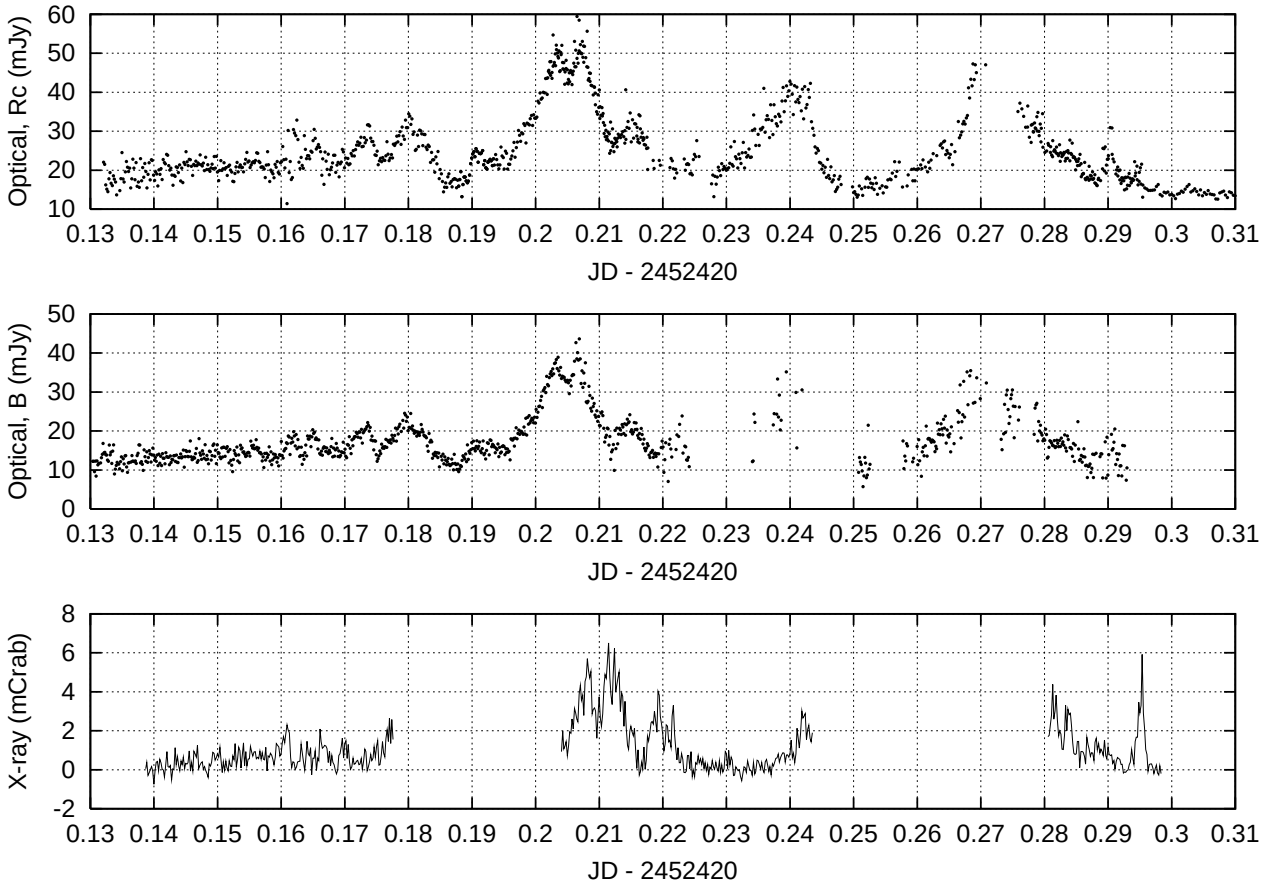

Fig. 5. Optical and X-ray light curves just after the outburst (JD 2452420). The abscissa and ordinate denote the time in JD and the flux density in mJy in the optical light curves and in mCrab in the X-ray light curve. Top panel: Optical R_c-band light curve. Middle panel: Optical B-band light curve. Interstellar extinction corrections were performed to these optical data. The typical error is 2.0 mJy in the R_c-band data and 1.5 mJy in the B-band data. Bottom panel: X-ray light curve. The typical error is 0.3 mCrab.

rapid fluctuations superimposed on the giant flare are more prominent in the X-ray light curve. In the optical range, the object became bluer and reached $B-R_c \sim 0.6$ at the peak. We obtain the de-reddened color of $B-R_c \sim 0.1$ with the reported reddening of $E(B-V) = 0.32$ (Orosz et al. 2001).

As well as this giant flare, we can see correlated X-ray–optical variations even in small flares around JD 2452420.15–2452420.18, in a rising to the second giant flare around JD 2452420.23–2452420.25, and in a short flare around JD 2452420.29–2452420.30. In Table 3, we present delay times calculated by cross-correlations. As shown in this table, the X-ray delay is typically ∼7 min, while the delay times have possible dispersions. The detection of the X-ray delay means that the optical emission was definitely not a reprocess of the X-ray emission. The table also shows marginal detection of B-band delays of about 20 s.

Simultaneous X-ray and optical observations were also performed on JD 2452421. The resulting light curves are shown in figure 6. The abscissa and ordinate are same as figure 5. The object was still active on JD 2452421. We can see a smaller optical flare in the upper panel of figure 6. Compared with flares on JD 2452420, the flare on JD 2452421 has a longer duration of ~ 1 hr and a larger e-folding time of rising branch of 62 ± 2 min.

Between JD 2452421.15–JD 2452421.16 in figure 6, our observation detected possible strong fluctuations superimposed on the more gradual trend of optical flare. We carefully checked images around these short-term variations and confirmed no change of transparency. At least one brightening which occurred at JD 2452421.154 was recorded in several images, which supports that they are real events.

In the X-ray range, a corresponding flare was also detected. It started rising at JD 2452421.152, which is about 24 min after the onset of the optical flare. An X-ray delay was hence observed also on JD 2452421 as well as the flares on JD 2452420, and furthermore, it became longer. This X-ray flare is characterized by strong fluctuations on the more gradual flare component. As can be seen in figure 6, the X-ray flux first increased rather smoothly, and then, the fluctuations became stronger with time. The fluctuation was strongest around JD 2452421.16 when the light curve was dominated by striking rapid brightenings. Some of them recorded over 20 mCrab. The X-ray peak

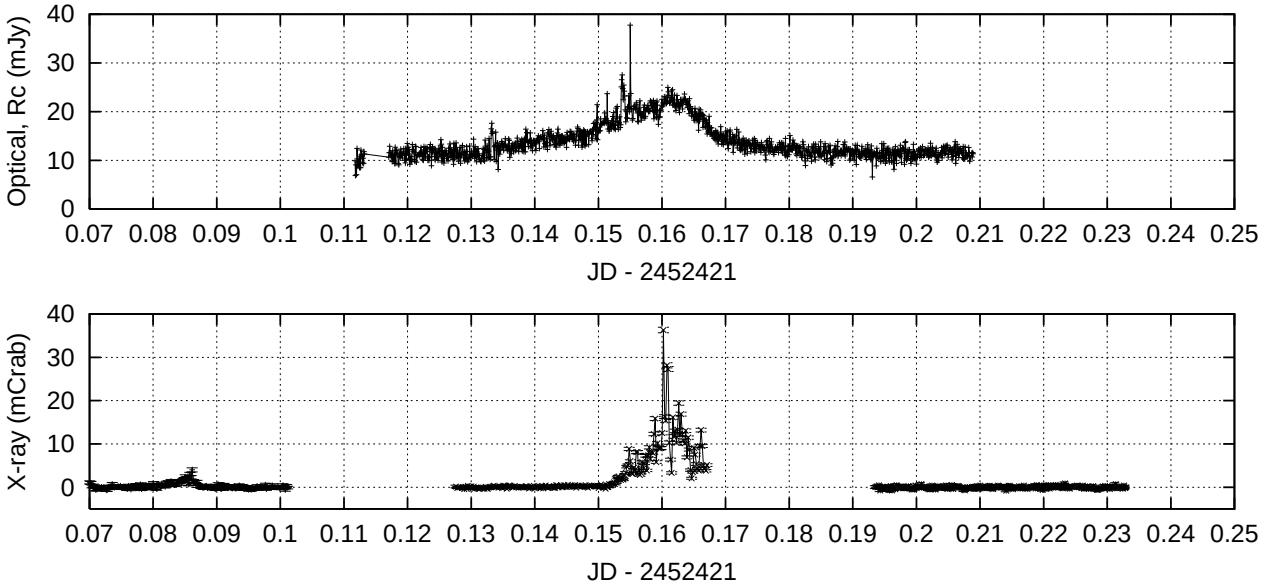

Fig. 6. Optical and X-ray light curves just after the outburst (JD 2452421). The abscissa and ordinate are same as figure 5. Upper panel: Optical R_c-band light curve. Interstellar extinction corrections were performed. The typical error is 1.1 mJy in the optical data. Bottom panel: X-ray light curve. The typical error is 0.2 mCrab during the low level and 0.4 mCrab during the flare.

luminosity on JD 2452421 is much higher than that on JD 2452420. The observed peak time of the X-ray flux roughly coincides with the optical peak. This is a notable difference compared with the flares on JD 2452420, in which both risings and peaks of the optical flares preceded those of the X-ray flux.

3.3. Active phase after the outburst

Our optical observations detected clear brightenings and fluctuations even after JD 2452421. They are shown in figure 7. A large flare with the peak magnitude of 12.2 mag was detected on JD 2452430, as shown in the panel (c) of figure 7. While its peak magnitude is comparable to those of flares observed on JD 2452420 and 2452421, the duration is much longer, at least 0.12 d. Other three panels (a, b, and d) show rapid variations with amplitudes smaller than 1 mag. They are rather minor, however evidently indicate that the object had remained active at least for two weeks after the outburst.

Figure 8 shows examples of power spectra of variations during and after the outburst. The abscissa and ordinate are the frequency in Hz and the power in an arbitrary unit. As can be seen in these power spectra, short-term variations of ~ 100 s still appeared after the outburst as well as ~ 1000 s variations. On JD 2452422, the object was calm throughout our observation for 0.17 d, as can be seen in the power spectrum in figure 8. It is, however, possible that a number of similar variations were overlooked due to their short durations. Within our available data, no other rapid variation with amplitudes over 0.2 mag was detected until JD 2452462, when the object again became active as reported in the next section.

3.3.1. Optical flash on July 7

On JD 2452462–2452463, the object exhibited sporadic, large-amplitude brightenings, as shown in figure 9, while it almost remained at the quiescent level except for the period of the brightenings. The activity became stronger with time; we can see brightenings with amplitudes of ~ 0.5 mag and durations of 100–500 s in the upper panel of figure 9, and then, remarkable rapid brightenings with a typical duration of 10–100 s in the lower panel. These "optical flashes" were superimposed on more gradual brightenings of about 0.5 mag. We cannot detect any periodicity in them.

The most prominent flash occurred around JD 2452463.165–2452463.167. During this flash, the object brightened to the maximum of 12.4 mag within 30 s, and then, returned to the pre-flash level within 90 s. Although the duration of the flash was very short, our observations successfully detected several points just during both ascending and descending branches, which provide unambiguous evidence for these variations. Figure 10 shows CCD images taken just before and during this flash. We can easily confirm the brightening at a high confidence level, comparing V4641 Sgr (the marked object) with neighbor stars. The optical flashes were detected only in the period shown in figure 9 and no similar variation was confirmed before and after this period.

As well as the optical flashes, several dips just before rapid brightenings are remarkable. Clear dips occurred at JD 2452463.130 and JD 2452463.165 just before the most prominent flash. We can see some another possible dips during the brightening periods, whereas no dip-like feature was detected when the object was at the quiescent level.

Radio observations show that no source was found on

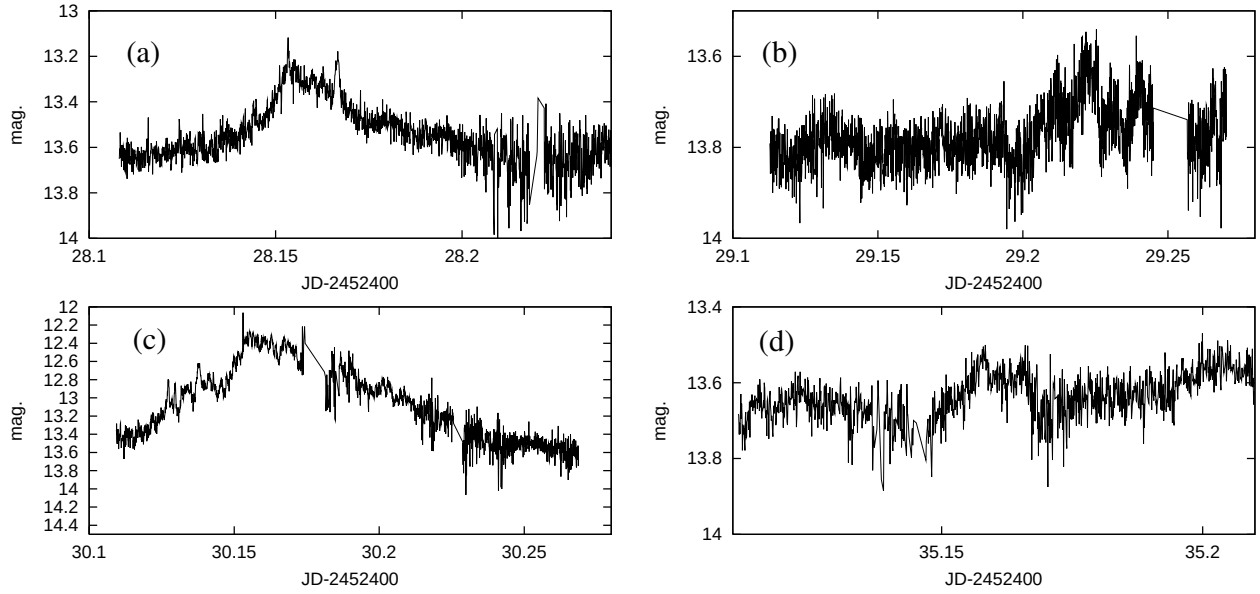

Fig. 7. Light curves showing rapid variations after the outburst. The abscissa and ordinate denote the time in JD and the R_c magnitude, respectively. The typical error is 0.04 mag in the panel (a), (b), and (d), and 0.07 mag in the panel (c). The power spectra of these variations are shown in figure 8.

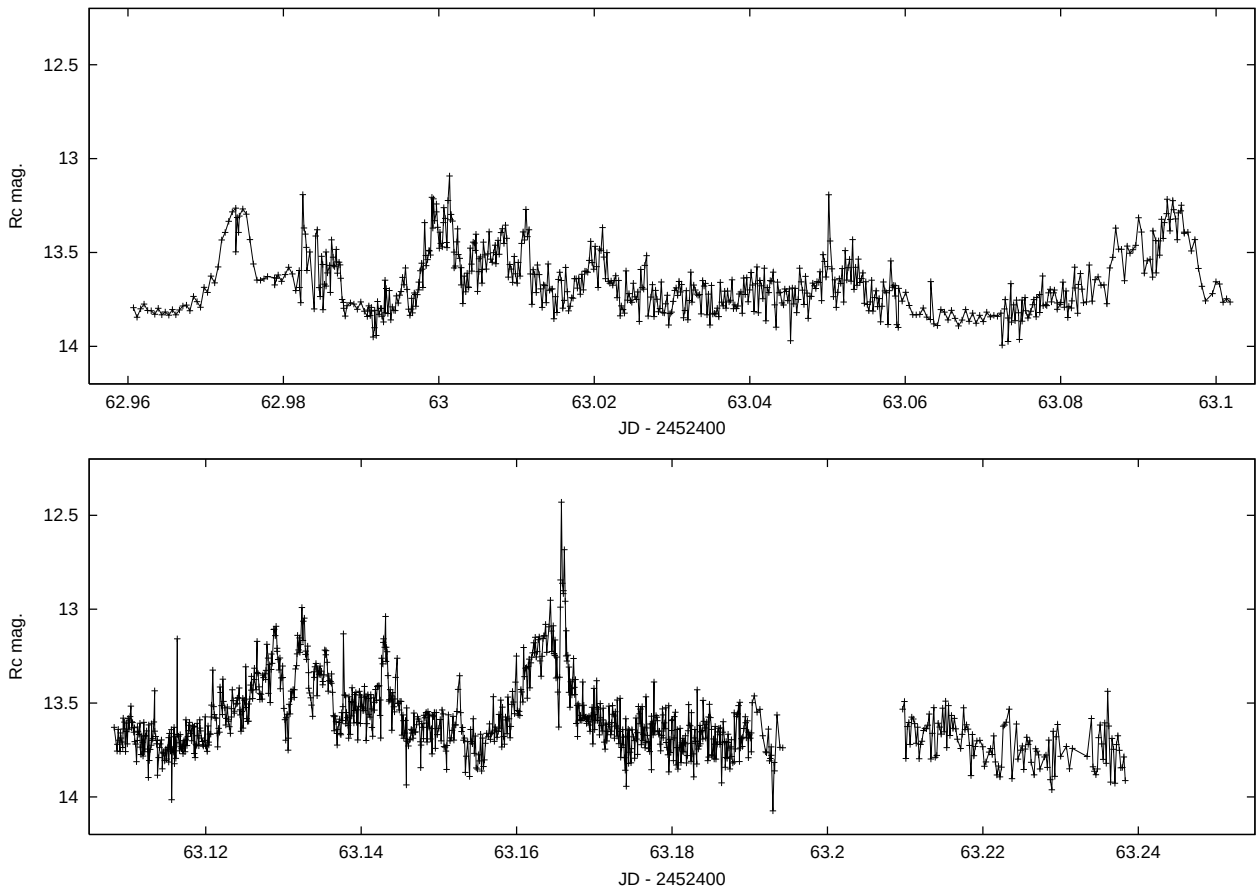

Fig. 9. Light curves of V4641 Sgr on 2002 July 7. The abscissa and ordinate denote the date and R_c magnitude, respectively. The error of each point is typically 0.05 mag.

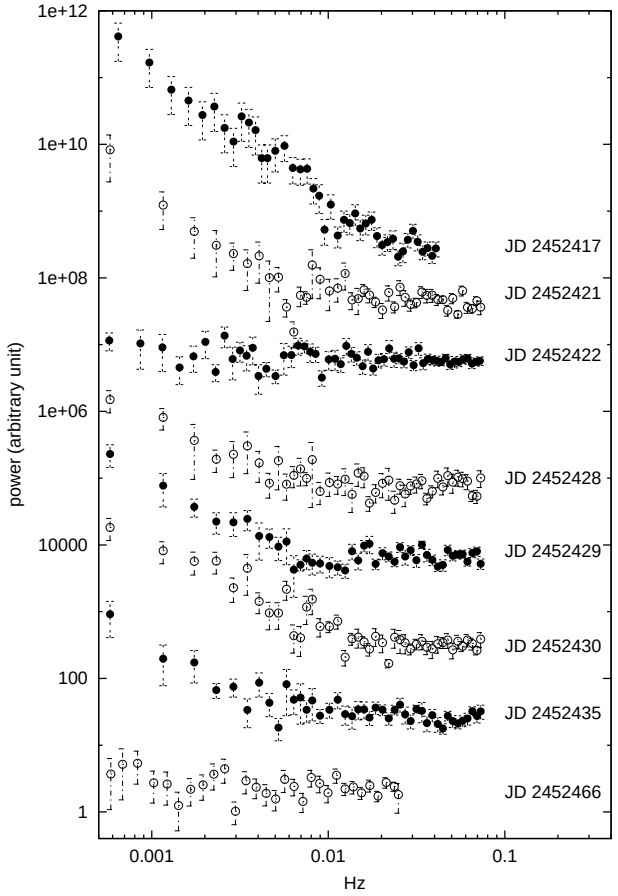

Fig. 8. Power spectra of optical short-term variations. The abscissa and ordinate are the frequency in Hz and the power in an arbitrary unit. The top points with the filled circles are a power spectrum during the outburst (JD 2452417). The other spectra are those after the outburst. The power spectra on JD 2452428–2452435 correspond to the short-term variations shown in figure 7.

June 5 at the position of V4641 Sgr. A radio source again appeared on July 13, and then, remained active on July 16, 24, 27, 28, and 29 (Rupen et al. 2002).[2] No X-ray observation is available around the optical flashes.[3] After JD 2452463, no short-term variation with amplitudes over 0.2 mag was detected within our available data. It was reported that the X-ray luminosity was lower than $10^{32}\,\mathrm{erg\,s^{-1}}$ on August 5, which indicates that the object had returned to the quiescent state (Tomsick et al. 2002).

3.4. Quiescent state

While several rapid brightenings were detected by our observation even after the May outburst, the object quickly returned to the quiescent level in the optical range just after the outburst. We performed period analysis using observations in 2002 combined with the past data reported in Uemura et al. (2002). The data contains 337-night observations from JD 2437109 to 2452569. We excluded light curves during the outburst or clearly showing rapid variations. Heliocentric corrections to the observed times were applied before the period analysis. Our period analysis with the phase dispersion minimization method (PDM; Stellingwerf 1978) yields the best period of $P = 2.817280 \pm 0.000015$ d, which is in agreement with the period reported in Uemura et al. (2002) and Orosz et al. (2001).

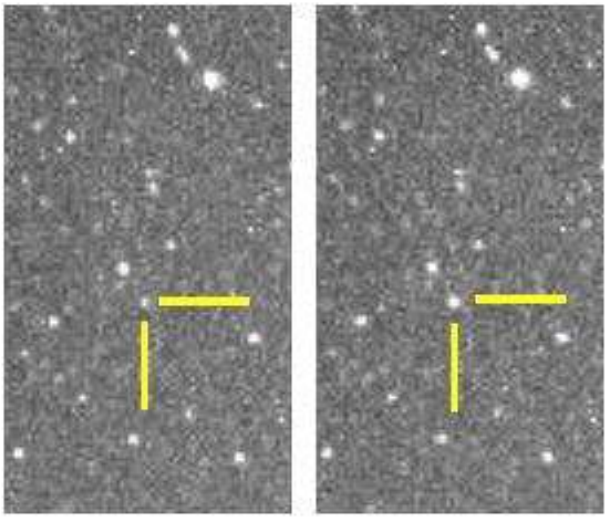

Fig. 10. CCD images of V4641 Sgr just before (left) and during (right) the giant optical flash. The images were observed at JD 2452463.16542 (left) and 2452463.16577. The time separation from the left to right images is 30 s. Each frame is $2'.5 \times 4'.3$; north is up and east to the left.

Figure 11 shows ellipsoidal modulations in 2002 June–October (JD 2452492–JD 2452569; filled circles) and in 1999–2001 (Uemura et al. 2002; open circles). As can be seen in the figure, the object exhibited ordinary ellipsoidal modulations after the outburst, as observed in 1999–2001. It is interesting to note that the object is possibly fainter around the secondary minimum after the May outburst, whereas the two maxima and the primary minimum are in agreement with those in 1999–2001. There is no significant difference in the average magnitude calculated from visual observations reported to VSNET between the period after the outburst and the period of 1999–2001.[4]

In figure 11, we also show three-night observations just before the May outburst with the filled crosses (JD 2452397, 2452406, and 2452407). Their brightness is consistent with the ordinary ellipsoidal modulation within the errors. This means that neither significant brightening nor fading was detected at least 13 d before the outburst. Visual observations reported to VSNET show the object was near the quiescent level at least 2 d before the outburst.

[2] ⟨http://vsnet.kusastro.kyoto-u.ac.jp/vsnet/Mail/vsnet-campaign-v4641sgr/msg00102.html, msg00104.html⟩

[3] ⟨http://xte.mit.edu/⟩

[4] ⟨http://vsnet.kusastro.kyoto-u.ac.jp/vsnet/index.html⟩

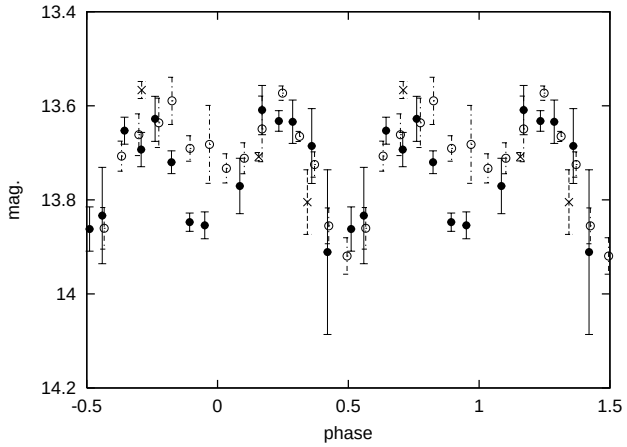

Fig. 11. Ellipsoidal modulations observed after the outburst in 2002 (filled circles) and 1999–2001 (open circles; Uemura et al. 2002). The abscissa denotes the phase calculated with the period of 2.81728 d and the epoch of HJD 2447708.89515 (Orosz et al. 2001). The ordinate denotes R_c-magnitude. The three crosses are observations in 2002, just before the outburst (JD 2452397, 2452406, and 2452407).

4. Discussion

4.1. Non-thermal optical emission during the outburst

Uemura et al. (2002) suggest the presence of non-thermal optical emission during the outburst of V4641 Sgr in May 2002 based on short time scales of variations and unusual colors. The optical SEDs around the outburst maximum (JD 2452419) are shown in figure 2. As can be seen in this figure, during the bin No. 7–11, the short-term variations became more prominent in the lightcurve and the flat spectral component became more dominant in the SEDs. As proposed in Uemura et al. (2002), the ~ 100 s variations definitely originated from the inner accretion region, where we cannot expect strong optical thermal emission. We conclude that the flat spectral component was caused by a strong contribution of the non-thermal emission, which was the source of short-term variations.

On the other hand, the object became bluer with the increase of the flux during the large flare. This property strongly indicates that the flaring component was thermal emission. The non-thermal short-term variations apparently became stronger with the decrease of the thermal flare.

Considering the significant contribution of the non-thermal emission even in B-band flux, we can estimate a lower limit of the temperature of the thermal component by calculating with de-reddened B and V-band flux. The temperature after the flare is estimated to be typically $\gtrsim 14000$ K. During this epoch, the contribution of the non-thermal component is more than 15% in R_c-band and 30% in I_c-band. On the other hand, at the peak of the flare (bin No. 3 in figure 2), the temperature of the thermal component is $\gtrsim 15000$ K. The non-thermal contribution is more than 10% in R_c-band and 25% in I_c-band. It should be noted that the non-thermal emission significantly contributes to R_c and I_c bands even at the peak of the flare.

The non-thermal optical emission is furthermore supported by the flat spectra in the radio range simultaneously taken with the optical observation on JD 2452419. In black hole binaries, flat or inverted radio spectra have been interpreted as evidence for self-absorbed synchrotron emission (Fender 2001). Such synchrotron emission has been proposed to possibly contribute to the optical emission (Fender 2001; Fender et al. 2001; Markoff et al. 2001). In the case of V4641 Sgr, based on i) the flat or inverted radio spectrum, ii) the positive detection of polarization shown in figure 3, and iii) the flat spectral component in the optical energy spectra shown in figure 2, we conclude that, around the outburst maximum, the wide range of the SED from the radio–optical region was dominated by strong synchrotron emission.

As well as JD 2452419, a flat radio spectrum was also reported on JD 2452418.[5]. On the other hand, the radio spectra just after the outburst were optically-thin synchrotron emission as shown in figure 4. The outburst may hence be characterized by long-lived strong synchrotron emission or frequent synchrotron flares which dominated in radio–optical wavelengths. On the other hand, there is also evidence for thermal flares, for example, the flare in figure 2 (and the flares just after the outburst, see the next section). It is possible that other multiple peaks during the outburst, as seen in the panel (a) of figure 1, were also a result of thermal flares. The complicated light curve of the May outburst is, hence, probably due to the increasing activity of both thermal and non-thermal sources, which must have an unknown relationship to each other.

4.2. X-ray delay of flares just after the outburst

In X-ray binaries, X-ray delays have been observed at onsets of X-ray nova outbursts (Orosz et al. 1997; Shahbaz et al. 1998; Uemura et al. 2002). They are interpreted as a result of the propagation of a heating wave from an outer accretion disk to the inner disk. The X-ray nova outburst starts at the outer, low temperature portion of the accretion disk, which first leads the optical brightening, and then, the propagation of the hot region into the inner, high temperature portion triggers the X-ray brightening later (Orosz et al. 1997; Hameury et al. 1997). This model has originally been developed for the UV delay phenomenon observed in dwarf novae (Livio, Pringle 1992; Meyer, Meyer-Hofmeister 1994). In the case of X-ray binaries, however, delay times are so long (a few days) compared with those in dwarf novae (a few hours) that another mechanism is required. Hameury et al. (1997) propose that the long delay times can be interpreted as a result of a longer propagation time into the inner, an advection dominated accretion flow (ADAF) region with a viscous time scale (Narayan, Yi 1994; Narayan et al. 1996). Based on the X-ray delay of order one day, the transition radius from the standard disk to the ADAF is estimated to be

[5] ⟨http://vsnet.kusastro.kyoto-u.ac.jp/vsnet/Mail/vsnet-campaign-v4641sgr/msg00037.html⟩

$\sim 10^4 r_{\rm g}$ during the quiescent state.

The properties of the optical and X-ray variations on JD 2452420 are summarized by i) the striking similarity of the light curves, ii) the 7-min X-ray delay, and iii) the shorter time scale of X-ray variations. The X-ray delay phenomenon at the onset of X-ray nova outbursts also have characteristics of i) and iii) (Orosz et al. 1997). We therefore conclude that the X-ray delay in V4641 Sgr can be also understood in terms of a hot region propagating into the inner portion of accretion flow. This simple picture should, however, be modified to explain the short time scale of the X-ray lag which is two orders shorter than those observed in other X-ray binaries.

Markwardt, Swank (2003) reported that the X-ray spectrum on JD 2452420 can be described not with a thermal disk, but with Compton scattering by a cold neutral medium. On the other hand, the source of the optical flares is probably a hot, thermal accretion component in the outer disk. We now consider a situation that this hot region propagates into the inner region with the viscous time scale. Using the equation (5) of Hameury et al. (1997) with same parameters (viscous parameter, $\alpha = 0.3$ and temperature, $T = 10^4$ K), the 7-min X-ray lag corresponds to the distance which the hot region travels, to be $\sim r_{\rm g}$, where $r_{\rm g}$ is the Schwarzschild radius. This small distance means that the hot region propagates in the standard disk to near the marginally stable orbit. Under such situation, we can generally expect strong thermal X-ray emission from the inner disk of the temperature about 10^7 K (Tanaka, Lewin 1995). In conjunction with the exceptionally low X-ray/optical flux ratio at the flare peak ($L_{\rm X}/L_{\rm opt} \sim 1$), the observed characteristics, that is, non-thermal and low luminosity X-ray emission, are inconsistent with the simple picture.

As well as the X-ray spectrum, the optical color is possibly inconsistent with the simple picture. Since the truncation radius is quite small, we need to consider the propagation of the hot region in the standard disk with the thermal time scale. The propagation speed of the hot region, v_f, can now be estimated with $v_f \sim \alpha c_{\rm s}$, where $c_{\rm s}$ is the sound speed in the hot region (Meyer 1984). Using the equation (1) in Hameury et al. (1997), we obtain the source of the optical flare at $< 5 \times 10^8$ cm ($= 170 r_{\rm g}$). It is a much inner region compared with the typical optical source at the outer accretion disk ($\sim 10^{10-11}$ cm). On the other hand, the temperature of the hot region can be estimated from the color. The de-reddened color of $B-V \sim 0.1$ indicates a hot region with the temperature of order 10^4 K, which is the typical temperature at the outer accretion disk during X-ray nova outbursts. Since the temperature in a standard disk strongly depends on the radius, it may hence be problematic that such inner region of $170 r_{\rm g}$ can produce flares of the low temperature of $\sim 10^4$ K.

With these discussions, it is evident that the simple picture with a propagating hot region must be improved to explain the observations. The short X-ray delay may require a propagation time shorter than the viscous or thermal time scale typical for black hole binaries. If we consider a significant contribution of non-thermal emission, as around the outburst maximum, the temperature of the flare may actually be much higher than $\sim 10^4$ K, which leads to a shorter thermal time scale. Although the radio observation shows the significant fading and the shift to the optically thin synchrotron emission 7 hours before the flare (see, figures 5 and 4), it is possible that a rapid radio flare occurred around the optical and X-ray flares, as detected during the outburst. It is also meaningful to consider a situation where a hot region falls with the free-fall time scale. If this is the case, the optical emission source can locate at outer region of $> 10^{10}$ cm. The ADAF can achieve such a situation, however, the size of the ADAF would be much larger than those proposed in other black hole binaries. An optically-thick advection dominated flow, or a slim disk, can also reproduce the rapid propagation. Revnivtsev et al. (2002) propose a similar situation to explain the outburst of V4641 Sgr in 1999. According to this model, the optical emission originated from an intervening medium absorbing/reprocessing X-rays, whose variation of size caused optical variations. A similar situation can explain the X-ray spectrum described with Compton scattering, and possibly the optical and X-ray variations in figure 5 and 6. In the case of the 2002 outburst and the active phase, however, the luminosity of the object was so low that we cannot expect the presence of a large, and long-lived super-critical accretion, or slim disk.

It is notable that the short X-ray delay was detected just after the outburst, when the object was presumably in a transition phase from the outburst to the quiescent state. The X-ray lag on JD 2452421 was longer than that on JD 2452420, which may imply that the object was just in a rapid state transition to the ordinary quiescent phase. The rising time scale of the flare was longer on JD 2452421 than that on JD 2452420. If the similar flare observed on JD 2452430 (the panel (c) of figure 7) has the same nature, we can say that the rising time scale was continuously increasing with time for about ten days. If the rising time scale corresponds to the propagation time of the hot region, the increase of the rising time scale may indicate the expansion of the accretion disk.

4.3. The peculiarity of the optical flash

Although optical short-term modulations were detected during the outburst in 2002 May, the optical flash on JD 2452462–2452463 has noteworthy characteristics. First, the object was not in a major outburst, but remained at the quiescent level around JD 2452463. During the outburst in May, the object experienced repeated short flares and the total duration was six days. On the other hand, variations like in figure 9 were observed only in this period and not on JD 2452461 and 2452464, which indicates a short duration of this active state. Second, no optical flash was detected during the May outburst. The ~ 100 s variations during the May outburst have amplitudes of order 0.1 mag, while the optical flash has amplitudes of 1.2 mag. The unique feature of the optical flash is the huge released energy only within the time scale of 10 s.

Using the peak apparent magnitude of $R_c = 12.4$ mag and the quiescent magnitude ($V = 13.8$), the optical luminosities are estimated to be $L_{\rm opt,peak} > 5.2 \times 10^{36}$ erg s^{-1} and $L_{\rm opt,quies} = 1.6 \times 10^{36}$ erg s^{-1}, respectively. In the above estimations, we assume an interstellar extinction of $A_V \sim 1.0$ and a distance of $d \sim 9.6$ kpc, which are reported in Revnivtsev et al. (2002) and Orosz et al. (2001). It should be noted that our observations with exposure times of 5 s may have overlooked more rapid variations and the real peak of the flash, and hence can only provide a lower limit of $L_{\rm opt,peak}$ in the above estimation. The peak released-energy rate of the flash component is then calculated to be $L_{\rm flash} > L_{\rm opt,flash} = L_{\rm opt,peak} - L_{\rm opt,quies} \gtrsim 4 \times 10^{36}$ erg s^{-1}, where $L_{\rm opt,flash}$ is the observed optical luminosity of the flash.

On the other hand, we can estimate a theoretical upper limit of the energy-release rate at a certain portion of an accretion disk. The observed optical emission on JD 2452463 indicates that the peak luminosity of the flash was much lower than that of the peak of its super-Eddington outburst in 1999 September (Uemura et al. 2002; Revnivtsev et al. 2002). The mass accretion rate was hence definitely smaller than the critical accretion rate ($\dot{M}_{\rm crit} \equiv L_{Edd}/\eta c^2$) throughout the active phase, where η is the energy conversion rate. We set a secure upper limit of the mass accretion rate to be $< 0.1 \dot{M}_{\rm crit}$ based on the optical peak luminosity of the flash. Under these assumptions, the observed energy release rate needs an emission source at

$$R_{\rm flash} < 150 (\frac{\eta}{0.1}) r_{\rm g}. \quad (1)$$

The radius of $150 r_{\rm g}$ corresponds to a dynamical time scale of 1 s. It is then possible that the optical flux was variable at 1-s scale during the active phase. Our visual observations indeed detected a very rapid variations of order 1 s and amplitudes of 0.3–0.9 mag during the active phase in 2002 May–July.[6] These observations may support the optical emission source at $< 150 r_{\rm g}$.

Such an inner emission source strongly indicates that the optical emission was non-thermal (Uemura et al. 2002). The optical flashes have a time scale shorter than that observed during the outburst in 2002 May, and hence, the scenario with synchrotron emission is even more preferable. The energy conversion rate in equation (1) strongly depends on the mechanism of the optical flash. When we consider a synchrotron optical flash, a part of gravitational energy is first transformed to magnetic energy, which then leads the acceleration of particles and generates synchrotron emission. The energy conversion rate should therefore be much smaller than 0.1 which is the value for the most effective disk. If we consider $\eta \sim 0.01$–0.001, it is possible that the optical flash is an event which occurred at the innermost region of the accretion flow.

When we consider the mechanism of the flash, it is interesting to note that the dips just before the flashes are also reported in the optical short-term variations in XTE J1118+480 (Kanbach et al. 2001; Spruit, Kanbach 2002). Both variations have a time scale of a few seconds, however, we should note that the released energy during the optical flash is much greater than those of rapid optical variations in XTE J1118+480 and GX 339−4 (Steiman-Cameron et al. 1997; Spruit, Kanbach 2002).

5. Summary

We observed V4641 Sgr during the outburst and post-outburst active phase in 2002 at optical, radio, and X-ray wavelengths. In the optical range, the object exhibited strong variations with a wide range of periods of 10^2–10^4 s. We conclude that ~ 1000 s, > 1 mag flares are thermal emission based on their bluer color and the X-ray lag. The 7-min X-ray lag is, however, too small to be interpreted in terms of a hot region propagating into the inner disk, as in the onset of X-ray nova outbursts. The short X-ray lag requires an unknown mechanism to account for the short propagation time of the hot region. On the other hand, the origin of short-term, ~ 100 s variations was presumably synchrotron emission. The flattening of the optical spectrum at the I_c, R_c, and V-band region strongly indicates a significant contribution of synchrotron emission even in the optical range. Their amplitudes are even relatively large (0.1–0.5 mag) compared with other black hole binaries showing optical rapid variations. Contrary to the current framework of the optical rapid variations, the optical flash, which was detected only on JD 2452462–2452463, has the unique and surprising characteristics that the object brightened by 1.2 mag only within 30 s. The released energy indicates that the flash occurred at the innermost region of the accretion flow. It should be noticed that dips were observed just before the flashes, as in XTE J1118+480.

To date, V4641 Sgr has continued to show us different features whenever it entered active phases. Considering the short duration of an active phase, we have possibly overlooked a number of other active phases. V4641 Sgr has almost all topics to which we have recently paid attention, for example, the disk–jet relationship, the broad Fe emission line in the X-ray range, the non-thermal optical emission, and the rapid optical variation. Therefore, close monitoring in all wavelength is strongly urged not only to reveal the nature of V4641 Sgr, but also to fully understand the accretion physics around the black hole.

We are grateful to many amateur observers for supplying their vital visual and CCD estimates via Variable Star Network (VSNET; http://vsnet.kusastro.kyoto-u.ac.jp/vsnet/). This work is partly supported by a grant-in aid from the Japanese Ministry of Education, Culture, Sports, Science and Technology (No. 13640239, 15037205). Part of this work is supported by a Research Fellowship of the Japan Society for the Promotion of Science for Young Scientists (MU and RI).

[6] ⟨http://vsnet.kusastro.kyoto-u.ac.jp/vsnet/Mail/vsnet-campaign-v4641sgr/msg00008.html,msg00026.html, msg00151.html ⟩

References

Abramowicz, M. A.; Kluzniak, W. 2001, A&A, 374, L19
Buie, M. W., & Bond, H. E. 1989, IAU Circ., 4786
Eikenberry, S. S., Matthews, K., Morgan, E. H., Remillard, R. A., & Nelson, R. W. 1998, ApJ, 494, L61
Fabian, A. C., Guilbert, P. W., Motch, C., Ricketts, M., Ilovaisky, S. A., & Chevalier, C. 1982, A&A, 111, L9
Fender, R. P. 2001, MNRAS, 322, 31
Fender, R. P., Hjellming, R. M., Tilanus, R. P. J., Pooley, G. G., Deane, J. R., Ogley, R. N., & Spencer, R. E. 2001, MNRAS, 322, L23
Frater, R. H., Brooks, J. W., & Whiteoak, J. B. 1992, J. Electrical and Electronics Engineering, Australia, 12, 103
Gotthelf, E., Patterson, J., & Stover, R. J. 1991, ApJ, 374, 340
Greiner, J., Morgan, E. H., & Remillard, R. A. 1996, ApJ, 473, L107
Hameury, J.-M., Lasota, J.-P., McClintock, J. E., & Narayan, R. 1997, ApJ, 489, 234
Hjellming, R. M. et al. 2000, ApJ, 544, 977
Hynes, R. I., Charles, P. A., Casares, J., Haswell, C. A., & Zurita, C.and Shabaz, T. 2003, MNRAS, accepted
Imamura, J. N., Kristian, J., Middleditch, J., & Steiman-Cameron, T. Y. 1990, ApJ, 365, 312
Jahoda, K., Swank, J. H., Giles, A. B., Stark, M. J., Strohmayer, T., Zhang, W., & Morgan, E. H. 1996, Proc. SPIE, 2808, 59
Kanbach, G., Straubmeier, C., Spruit, H. C., & Belloni, T. 2001, Nature, 414, 180
Livio, M., & Pringle, J. E. 1992, MNRAS, 259, 23
Markoff, S., Falcke, H., & Fender, R. 2001, A&A, 372, L25
Markwardt, C. B., & Swank, J. H. 2003, in preparation
Merloni, A., Di Matteo, T., & Fabian, A. C. 2000, MNRAS, 318, L15
Meyer, F. 1984, A&A, 131, 303
Meyer, F., & Meyer-Hofmeister, E. 1994, A&A, 188, 175
Mirabel, I. F., Dhawan, V., Chaty, S., Rodriguez, L. F., Marti, J., Robinson, C. R., Swank, J., & Geballe, T. 1998, A&A, 330, L9
Morgan, E. H., Remillard, R. A., & Greiner, J. 1997, ApJ, 482, 993
Motch, C., Ilovaisky, S. A., & Chevalier, C. 1982, A&A, 109, L1
Motch, C., Ilovaisky, S. A., Chevalier, C., & Angebault, P. 1985, Space Sci. Rev., 40, 219
Motch, C., Ricketts, M. J., Page, C. G., Ilovaisky, S. A., & Chevalier, C. 1983, A&A, 119, 171
Narayan, R., McClintock, J. E., & Yi, I. 1996, ApJ, 457, 821
Narayan, R., & Yi, I. 1994, ApJ, 428, L13
O'Donoghue, D., & Charles, P. A. 1996, MNRAS, 282, 191
Orosz, J. A. et al. 2001, ApJ, 555, 489
Orosz, J. A., Remillard, R. A., Bailyn, C. D., & McClintock, J. E. 1997, ApJL, 478, L83
Rao, A. R., Naik, S., Vadawale, S. V., & Chakrabarti, S. K. 2000, A&A, 360, L25
Revnivtsev, M., Sunyaev, R., Gilfanov, M., & Churazov, E. 2002, aap, 385, 904
Rupen, M. P., Dhawan, V., & Mioduszewski, A. J. 2002, IAU Circ., 7928
Sams, B. J., Eckart, A., & Sunyaev, R. 1996, Nature, 382, 47
Shahbaz, T., Bandyopadhyay, R. M., Charles, P. A., Wagner, R. M., Muhli, P., Hakala, P., Casares, J., & Greenhill, J. 1998, MNRAS, 300, 1035
Smith, D. A., Levine, A. M., & Morgan, E. H. 1999, IAU Circ., 7253
Spruit, H. C., & Kanbach, G. 2002, A&A, 391, 225
Steiman-Cameron, T., Imamura, J., Middleditch, J., & Kristian, J. 1990, ApJ, 359, 197
Steiman-Cameron, T. Y., Scargle, J. D., Imamura, J. N., & Middleditch, J. 1997a, ApJ, 487, 396
Steiman-Cameron, T. Y., Scargle, J. D., Imamura, J. N., & Middleditch, J. 1997b, ApJ, 487, 396
Stellingwerf, R. F. 1978, ApJ, 224, 953
Taam, R. E., Chen, X., & Swank, J. H. 1997, ApJ, 485, L83
Tanaka, Y., & Lewin, W. H. G. 1995, in X-Ray Binaries, ed. W. H. G. Lewin, J. van Paradijs & van den Heuvel. E. P. J. (Cambridge University Press, Cambridge)
Taylor, B. J. 1986, ApJS, 60, 577
Tomsick, J. A. et al. 2002, ATEL, 105
Uemura, M. et al. 2002a, PASJ, 54, L79
Uemura, M. et al. 2002b, PASJ, 54, 285
Uemura, M., Kato, T., Watanabe, T., Stubbings, R., Monard, B., & Kawai, N. 2002c, PASJ, 54, 95
van der Klis, M. 1989, ARA&A, 27, 517
Wagner, R. M., Kreidl, T. J., Howell, S. B., Collins, G. W., & Starrfield, S. 1989, IAU Circ., 4797
Wei, C., Zhang, S. N., & Chen, W. 1998, ApJ, 492, L53
Wei, C., Zhang, S. N., Focke, W., & Swank, J. H. 1997, ApJ, 484, 383
Yadav, J. S., Rao, A. R., Agrawal, P. C., Paul, B., Seetha, S., & Kasturirangan, K. 1999, ApJ, 517, 935

Table 1. Observation log

$T_{\rm start}$ (HJD)	ΔT (hr)	$T_{\rm exp}$	N	Filter	Site
2452397.281	0.53	10	117	–	Kyoto
2452406.264	0.20	10	38	–	Kyoto
2452407.297	0.18	10	37	–	Kyoto
2452415.398	6.41	10	237	–	Bronberg
2452415.667	6.33	120	8	V	Cerro Tololo
2452415.908	0.65	15	18	V	Mulvane
2452415.913	0.24	30	14	V	Mulvane
2452416.248	1.37	10	261	–	Kyoto
2452416.296	9.05	10	904	–	Bronberg
2452416.742	1.85	120	24	V	Cerro Tololo
2452416.913	0.62	30	35	–	Mulvane
2452417.544	3.00	10	948	–	Bronberg
2452417.665	4.94	120	23	V	Cerro Tololo
2452417.916	0.46	30	26	–	Mulvane
2452418.202	1.82	1	1780	$R_{\rm c}$	Ouda
2452418.208	1.30	5	454	–	Okayama
2452418.246	0.69	10	115	–	Kyoto
2452418.383	2.11	10	293	–	Bronberg
2452419.022	2.14	15	203	V	Ellinbank
2452419.086	4.85	30	137	$I_{\rm c}$	Tsukuba
2452419.087	4.80	130	192	V	Tsukuba
2452419.096	3.03	10	698	–	Kyoto
2452419.114	0.10	1	112	$R_{\rm c}$	Ouda
2452419.119	4.32	1	5417	B	Ouda
2452419.140	3.84	3	1558	–	Okayama
2452419.163	3.37	10	740	–	Kyoto
2452419.183	2.50	130	55	B	Tsukuba
2452419.298	2.26	10	273	–	Bronberg
2452419.986	2.04	15	371	–	Woodridge
2452420.083	1.61	10	46	–	Tahiti
2452420.120	0.05	1	76	$R_{\rm c}$	Ouda
2452420.123	4.06	10	925	B	Ouda
2452420.137	2.05	10	471	–	Kyoto
2452420.207	2.34	10	390	–	Kyoto
2452420.275	8.47	10	1014	–	Bronberg
2452421.111	3.14	5	1206	$R_{\rm c}$	Ouda
2452421.272	9.12	10	755	–	Bronberg
2452422.113	4.13	5	2138	$R_{\rm c}$	Ouda
2452422.125	4.14	10	868	–	Kyoto
2452422.125	4.14	10	871	–	Kyoto
2452424.067	3.51	10	364	–	Kyoto
2452424.126	4.01	5	1370	$R_{\rm c}$	Ouda
2452424.523	3.58	10	478	–	Bronberg
2452426.483	2.71	15	540	–	Ceccano
2452428.108	3.89	5	1725	$R_{\rm c}$	Ouda
2452428.131	2.93	10	405	–	Kyoto
2452429.112	3.79	5	1813	$R_{\rm c}$	Ouda
2452430.109	3.82	5	1810	$R_{\rm c}$	Ouda
2452430.561	2.50	5	723	–	Okayama
2452431.065	5.60	10	1027	–	Kyoto
2452431.065	5.60	10	1037	–	Kyoto
2452432.065	5.19	10	809	–	Kyoto
2452432.112	2.57	5	593	–	Okayama
2452435.097	2.94	10	372	–	Kyoto
2452435.111	2.35	5	1157	$R_{\rm c}$	Ouda

$T_{\rm exp}$: Exposure time, N: Number of frame

Table 1. (Continued)

$T_{\rm start}$ (HJD)	ΔT (hr)	$T_{\rm exp}$	N	Filter	Site
2452437.065	2.16	30	112	$I_{\rm c}$	Tsukuba
2452437.988	4.42	30	175	$I_{\rm c}$	Tsukuba
2452437.989	3.79	80	82	V	Tsukuba
2452439.211	1.01	5	142	$R_{\rm c}$	Ouda
2452439.989	3.79	80	82	V	Tsukuba
2452440.017	4.32	30	176	$I_{\rm c}$	Tsukuba
2452440.068	0.14	30	14	B	Tsukuba
2452441.070	3.86	10	566	–	Kyoto
2452442.009	3.17	130	70	$I_{\rm c}$	Tsukuba
2452442.012	2.83	30	124	V	Tsukuba
2452445.093	0.67	30	58	V	Tsukuba
2452453.076	1.49	5	407	–	Okayama
2452454.473	–	5	200	V	Crimea
2452455.403	–	5	200	V	Crimea
2452456.044	1.01	10	300	V	Nayoro
2452457.996	5.72	10	339	–	Kyoto
2452458.407	0.60	200	5	V	Crimea
2452459.394	0.55	200	5	V	Crimea
2452461.359	1.63	200	13	V	Crimea
2452462.350	1.82	200	13	V	Crimea
2452462.956	3.38	20	166	–	Tahiti
2452462.979	6.35	10	515	–	Kyoto
2452463.078	2.90	20	255	–	Wako
2452463.114	2.11	5	654	–	Okayama
2452463.347	1.85	200	13	V	Crimea
2452464.213	9.41	10	993	–	Bronberg
2452464.342	2.42	20	300	V	Crimea
2452465.048	0.22	5	88	V	Nayoro
2452466.297	7.56	10	1057	–	Bronberg
2452466.649	0.30	5	100	–	Seikei
2452466.978	6.41	10	655	–	Kyoto
2452467.004	2.54	15	462	–	Wako
2452467.909	6.67	15	1199	–	Woodridge
2452467.959	4.41	10	467	–	Kyoto
2452468.077	2.90	15	264	–	Wako
2452468.423	1.82	7	722	–	Ceccano
2452468.895	3.96	20	360	–	Tahiti
2452469.284	7.68	10	1086	–	Bronberg
2452471.964	4.94	5	738	$R_{\rm c}$	Ouda
2452471.982	4.01	10	258	–	Kyoto
2452472.011	2.38	15	274	–	Wako
2452475.972	0.80	10	117	–	Kyoto
2452476.061	3.43	5	513	–	Wako
2452476.971	5.67	10	787	–	Kyoto
2452479.048	1.49	10	453	–	Kyoto
2452480.984	5.20	10	683	–	Kyoto
2452481.985	4.94	10	713	–	Kyoto
2452491.954	5.09	10	1120	–	Kyoto
2452492.959	4.68	10	807	–	Kyoto
2452493.969	4.33	10	872	–	Kyoto
2452496.124	0.63	10	137	–	Kyoto
2452497.949	4.47	10	790	–	Kyoto
2452498.957	0.74	10	155	–	Kyoto
2452499.952	4.46	10	903	–	Kyoto
2452502.968	4.18	10	820	–	Kyoto

$T_{\rm exp}$: Exposure time, N: Number of frame

Table 1. (Continued)

$T_{\rm start}$ (HJD)	ΔT (hr)	$T_{\rm exp}$	N	Filter	Site
2452508.944	3.65	10	365	–	Kyoto
2452511.954	3.67	10	684	–	Kyoto
2452512.935	2.30	10	405	–	Kyoto
2452515.047	1.20	10	258	–	Kyoto
2452515.952	3.30	10	701	–	Kyoto
2452516.936	3.62	10	662	–	Kyoto
2452518.937	3.68	10	817	–	Kyoto
2452519.934	3.64	10	571	–	Kyoto
2452522.928	3.43	10	704	–	Kyoto
2452525.929	3.38	10	716	–	Kyoto
2452526.914	3.78	10	798	–	Kyoto
2452535.915	2.73	10	554	–	Kyoto
2452536.912	2.96	10	493	–	Kyoto
2452537.926	2.07	10	141	–	Kyoto
2452540.907	2.80	10	615	–	Kyoto
2452541.944	2.93	10	556	–	Kyoto
2452557.880	2.33	10	513	–	Kyoto
2452558.899	1.74	10	362	–	Kyoto
2452559.922	0.98	10	203	–	Kyoto
2452560.883	2.08	10	454	–	Kyoto
2452561.873	2.26	10	498	–	Kyoto
2452563.882	2.02	10	446	–	Kyoto
2452564.876	1.67	10	362	–	Kyoto
2452568.882	1.29	10	234	–	Kyoto
2452569.871	1.57	10	299	–	Kyoto

$T_{\rm exp}$: Exposure time, N: Number of frame

Table 2. Radio spectral index

JD−2452420	α (from all data)	α (from 3 high frequencies)
9.003	0.11± 0.05	0.05± 0.09
9.020	0.20± 0.09	0.27± 0.16
9.038	0.38± 0.12	0.54± 0.17
9.057	0.58± 0.12	0.77± 0.12
9.076	0.70± 0.12	0.89± 0.04
9.094	0.81± 0.09	0.97± 0.02
9.321	0.25± 0.14	0.03± 0.09
9.339	0.23± 0.12	0.05± 0.10
9.357	0.16± 0.12	-0.04± 0.08
9.372	-0.20	-0.20
9.928	-0.25± 0.09	-0.34± 0.16
10.934	-0.66± 0.09	-0.66± 0.09

Table 3. X-ray and B-band flux delays against $R_{\rm c}$-band flux calculated with cross-correlations.

JD−2452420	X-ray−Optical($R_{\rm c}$) (min)	X-ray−Optical(B) (min)	Optical(B)−Optical($R_{\rm c}$) (min)
0.15–0.18	5.67 ± 0.98	6.40 ± 0.70	0.34 ± 0.21
0.19–0.23	7.25 ± 0.42	7.01 ± 0.37	0.29 ± 0.19
0.28–0.30	—	6.85 ± 0.72	—